Nuclear Instruments and Methods in Physics Research B 282 (2012) 88–91

Contents lists available at SciVerse ScienceDirect

Nuclear Instruments and Methods in Physics Research B

journal homepage: www.elsevier.com/locate/nimb

Ion-beam synthesis and photoluminescence of SiC nanocrystals assisted by MeV-heavy-ion-beam annealing

J. Khamsuwan [a], S. Intarasiri [b], K. Kirkby [c], P.K. Chu [d], S. Singkarat [a,e], L.D. Yu [a,e,*]

[a] Plasma and Beam Physics Research Facility, Department of Physics and Materials Science, Faculty of Science, Chiang Mai University, Chiang Mai 50200, Thailand
[b] Science and Technology Research Institute, Chiang Mai University, Chiang Mai 50200, Thailand
[c] Surrey Ion Beam Centre, University of Surrey, Guildford, Surrey GU2 7XH, UK
[d] Department of Physics and Materials Science, City University of Hong Kong, Tat Chee Avenue, Kowloon, Hong Kong, China
[e] Thailand Center of Excellence in Physics, Commission on Higher Education, 328 Si Ayutthaya Road, Bangkok 10400, Thailand

ARTICLE INFO

Article history:
Available online 16 September 2011

Keywords:
Heavy-ion-beam annealing (HIBA)
Silicon carbide (SiC)
Ion beam synthesis
Ion implantation
Photoluminescence

ABSTRACT

This work explored a novel way to synthesize silicon carbide (SiC) nanocrystals for photoluminescence. Carbon ions at 90 keV were implanted in single crystalline silicon wafers at elevated temperature, followed by irradiation using xenon ion beams at an energy of 4 MeV with two low fluences of 5×10^{13} and 1×10^{14} ions/cm^2 at elevated temperatures for annealing. X-ray diffraction, Raman scattering, infrared spectroscopy and transmission electron microscopy were used to characterize the formation of nanocrystalline SiC. Photoluminescence was measured from the samples. The results demonstrated that MeV-heavy-ion-beam annealing could indeed induce crystallization of SiC nanocrystals and enhance emission of photoluminescence with violet bands dominance due to the quantum confinement effect.

1. Introduction

Silicon carbide (SiC) is highly attractive in electronic devices for high-temperature, high-frequency and high-power applications rather than silicon because of its excellent properties such as wide band gap, high-temperature stability, high thermal conductivity, radiation hardness and chemical inertness [1]. However, it is hard and complicated to grow high-quality large areas of SiC [2,3], and hence synthesis of industrially applicable SiC crystals has widely been studied [4]. Ion beam synthesis has been one of the methods studied to produce a homogeneous polycrystalline SiC layer buried in silicon single crystals with some advantages [4,5]. This approach applies high-fluence carbon ion implantation in silicon in combination with either subsequent or *in situ* thermal annealing to crystallize SiC [4,6,7]. With this method high-quality large-area SiC ready for device fabrication can be produced but a high annealing temperature, up to more than 1000 °C, is normally required. High-energy heavy-ion-beam annealing (HIBA) has recently appeared to be an alternative to thermal annealing using moderate temperatures for crystallization of SiC induced by ion implantation [7,8]. As a newly developed technique, high-energy HIBA has plenty of potentials to be applied more extensively. In this study we used an MeV xenon ion beam for the annealing purpose to synthesize nanocrystalline SiC and investigate related effects, particularly, on the photoluminescence of thus formed SiC.

2. Experiment

Samples of 2-in. (100) p-type Si wafers were implanted with 90-keV carbon ions to a fluence of 6.5×10^{17} ions/cm^2 at an elevated temperature of 400 °C. The C-ion fluence was chosen to achieve a stoichiometric C–Si in the implanted layer for forming SiC. The sample temperature was applied based on the technical upper limit of the heating method which used a 250 W halogen lamp to heat the sample from the backside. After C-ion implantation, the samples were irradiated by 4-MeV $^{131}Xe^{2+}$ ions to fluences of 5×10^{13} and 1×10^{14} ions/cm^2 at a target sample temperature of 500 °C for HIBA. The elevated sample temperature was determined from our previous tests [7] which showed that appropriately medium sample temperatures during HIBA could be effectively assistant to the crystallization of SiC, whereas lower temperatures did not work and higher temperatures were not necessary. In order to carefully control the ion beam annealing effect on the sample to eliminate possible errors, in the HIBA process three parts of the C-ion implanted Si wafer were treated in such a way that the lower half was shielded from the ion beam, the upper part was implanted to a fluence of 5×10^{13} ions/cm^2 and then half of the upper part was shielded again but ions were continued to implant to another half of the upper part to a final fluence of 1×10^{14} ions/cm^2. After MeV Xe-HIBA, the wafer was cut into

* Corresponding author at: Plasma and Beam Physics Research Facility, Department of Physics and Materials Science, Faculty of Science, Chiang Mai University, Chiang Mai 50200, Thailand.
E-mail address: yuld@fnrf.science.cmu.ac.th (L.D. Yu).

0168-583X/$ - see front matter © 2011 Elsevier B.V. All rights reserved.
doi:10.1016/j.nimb.2011.08.058

1 cm × 1 cm sample pieces for characterization. The formation of SiC was characterized using X-ray diffraction (XRD) (a Philips X'Pert system using Cu K_α radiation at 40 kV, 30 mA and step size of 0.05°), Fourier transformation infrared (FTIR) spectroscopy (a Perkin Elmer Fourier-transform infrared spectrometer in the range of 400–1500 cm^{-1} with a resolution of 4 cm^{-1}), Raman scattering (Renishaw 2000, with argon laser excitation at 514 nm in backscattering configuration), and transmission electron microscopy (TEM). Rutherford backscattering spectrometry (RBS) (2.13-MeV He^{2+} beam, 160° backscattering angle) and elastic (non-Rutherford) backscattering (EBS) (1.734 MeV H^+ beam, 173° backscattering angle) analyses were performed for carbon depth profile information. A photoluminescence (PL) measurement of the SiC layer in the samples, which were ion-beam-sputtered by reactive ion etching under O_2 and SF_6 plasma with 30 torr to remove the top layer, was operated under the excitation of 337 nm N_2 laser line at room temperature.

3. Results and discussion

Figs. 1 and 2 show XRD and TEM evidence of the MeV Xe-HIBA induced formation of nanocrystalline SiC buried in Si. Since the X-ray energy of Cu K_α was nearly 8 keV, it could completely penetrate about 0.5 mm of Si, and thus the XRD information should come from the entire implanted C region which was about 100–500 nm below the top surface as shown by the result on the C depth profile below. In the XRD spectra one sees clearly the diffraction peaks of 3C–SiC or β-SiC (200), (400), and the peak of the silicon substrate (400) at about 41.4°, 89.2°, and 69.1°, respectively [6,7,9]. In a comparison in the XRD spectra between the C-ion as-implanted Si and Xe-HIBA C-ion-implanted Si, it is obvious that the SiC peaks after HIBA are present or considerably higher whereas in the as-implanted case there are either no SiC peaks or almost negligible peaks, indicating that the HIBA certainly induces or promotes the formation of SiC. The HIBA also shows an effect on recrystallization of Si as shown by the fact that the Si peak after HIBA is higher and sharper than the as-implanted peak. The recrystallization is sensitive to the annealing beam fluence as shown by the difference in the Si peak height between the two fluences. When the annealing beam fluence is higher, more damage may be introduced and thus the recrystallization effect is not as pronounced as the lower fluence. The TEM image shows that while the as-implanted area is nearly amorphous, the HIBA causes formation of SiC nanocrystals in sizes of about several nanometers, which is in a good agreement with the calculated size of about 9 nm from the (200) peak and 6 nm from the (400) peak in the XRD spectra using the Scherrer formula [10]. The Si recrystallization induced by the MeV Xe-HIBA is also demonstrated in the TEM image.

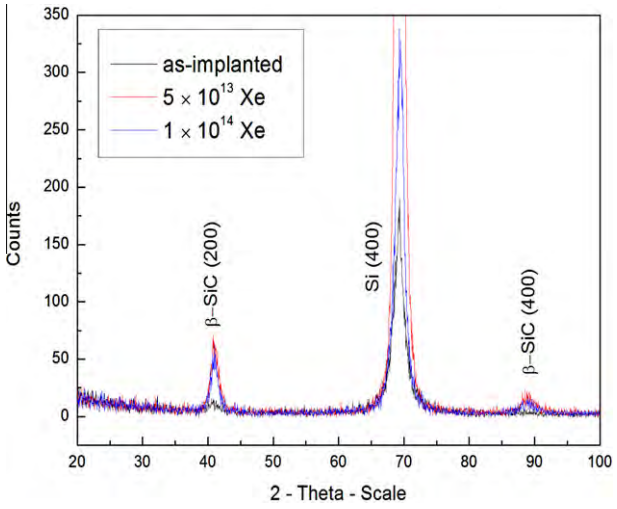

Fig. 1. XRD spectra of the C-ion as-implanted Si sample and the samples after C-ion implantation in Si followed by MeV-Xe HIBA.

The chemical bonding between the silicon and carbon atoms in the SiC layer was investigated by FTIR absorption measurements as shown in Fig. 3. As long-wavelength IR radiation could penetrate normal materials deeply, such as many micrometers to millimeters, the IR information should reflect the physics and chemistry in the whole implanted C region. An unimplanted silicon wafer was used to measure the background signal which had been subtracted from the spectra. Peaks located at a wavenumber of ~796 cm^{-1} are obviously seen in all the spectra, and this wavenumber is corresponding to the transversal optical (TO) phonon absorption of crystalline β-SiC [11–13]. The 796-cm^{-1} peak significantly becomes sharper and stronger after Xe-HIBA with a transmittance decrease of about 50% or an absorption increase over 100%. This fact clearly demonstrates the role played by the HIBA in crystallizing SiC. On the as-implanted spectrum, a small broad bump is present at about 750 cm^{-1}, which is related to the presence of an amorphous SiC phase in the implanted layer [13]. After Xe-HIBA to both fluences, the small bump at 750 cm^{-1} disappears along with the drastic increase in the intensity of the 796-cm^{-1} peak, indicating crystallization of SiC by the MeV Xe-HIBA.

Raman-scattering measurements were also performed to provide information, which was comparatively weak [5], to bear further evidence of the crystalline SiC formation, as shown in Fig. 4. The spectrum from the as-implanted sample shows a peak at 520 cm^{-1} corresponding to the longitudinal optical (LO) phonon mode of absorption of the crystalline Si [14] and the Si second-order peak at 970 cm^{-1}. In all cases, while the peaks at 520 cm^{-1} are still clear, the peaks at 970 cm^{-1} become less prominent after the Xe-HIBA. This phenomenon may imply that the silicon at the top surface (compared with the IR radiation, laser radiation used in Raman scattering deals with only the top layer) becomes somehow amorphous by the MeV Xe-ion bombardment. On the spectrum of the high-fluence Xe-HIBA sample, although Raman scattering is a weak interaction between photons and phonons and thus sometimes comparatively not very sensitive, a small bump appears very near 800 cm^{-1}. This indicates the formation of 3C–SiC as the TO mode of 3C–SiC is at ~796 cm^{-1} [7,15].

The mechanism of the high-energy HIBA effect on crystallization of SiC has been attributed to electronic stopping [7]. The electronic stopping dominates the incident high-energy ion's high energy loss process which takes place in the distribution region of the implanted carbon in Si (the range of 4-MeV Xe in Si is about 1 μm, while the C ions are distributed mostly in 200–350 nm, as shown below). The electron–phonon interaction deposits the ion energy for the purpose of annealing. To compare with our previous study using tens-MeV I-HIBA with lower fluences [7], we this time used an MeV Xe-ion beam with higher fluences for searching roles in annealing played by relevant factors such as ion energy and fluence. It is found that the HIBA effect on crystallization of SiC crucially depends on the ion energy but not the areal ion energy density (the product of ion energy and fluence) deposited in the material [16]. Our previous study demonstrated that the crystallization of SiC was solely caused by HIBA but only the elevated sample temperature of 500 °C did not anneal anything [7].

Fig. 5 displays the C-ion depth profiles extracted from the EBS and RBS spectra measured before and after the Xe-HIBA. The extraction of the real C-ion profiles from EBS and RBS spectra was performed using both the DataFurnace code [17] and a self-developed software [18], which took use of the deficient part of the RBS spectrum of a light element implanted heavy matrix or

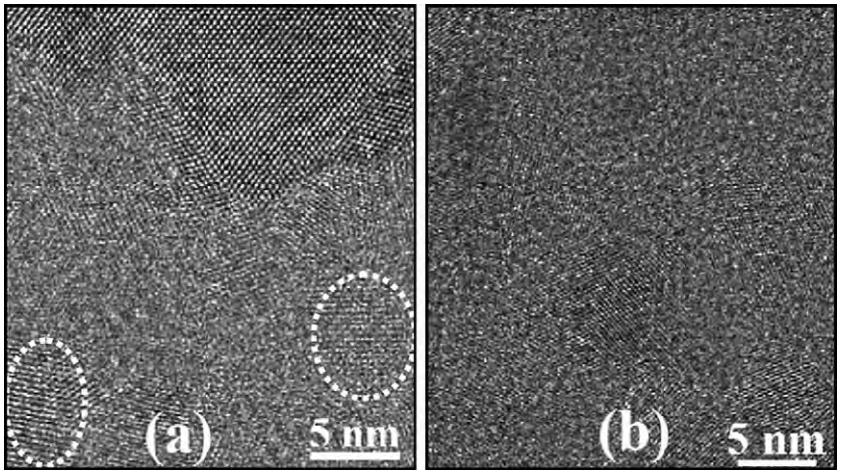

Fig. 2. High resolution TEM images of the C-ion implanted area in Si (a) after and (b) before the MeV-Xe HIBA. The image in (a) is at the interface of the C-ion implanted area (lower part) and the Si layer (upper part) above the implanted C layer, and so recrystallized Si can be seen at the upper part. SiC nanocrystals are indicated by dashed circles.

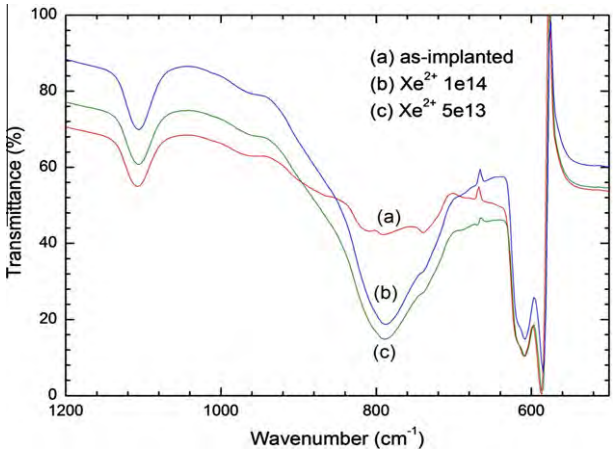

Fig. 3. IR transmittance spectra from Xe-ion-beam annealed and as-implanted samples.

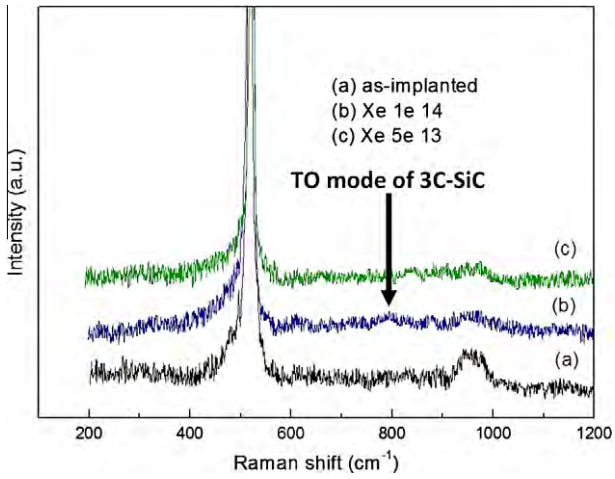

Fig. 4. Raman spectra from Xe-ion-beam annealed and as-implanted samples.

the extraction and also accounted for the depth dependent compositions of the material. In general, the measured C-ion depth profiles reasonably agree with the one simulated with SRIM [19] in basic parameters such as the range, range straggling and maximum concentration. A small profile shift is observed due to the HIBA. The

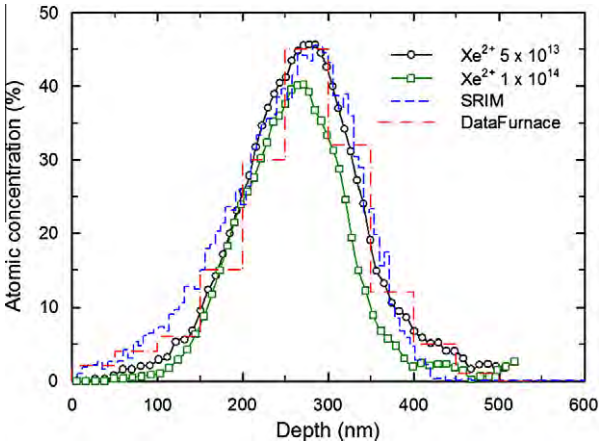

Fig. 5. Depth distributions of atomic concentration of 90-keV C ions implanted in Si before and after 4-MeV Xe-ion beam annealing analyzed by EBS, RBS and SRIM simulation. The SRIM-simulated and DataFurnace-calculated profiles are without ion beam annealing.

C profile after the lower-fluence Xe-ion beam annealing has a very slight, almost negligible, shift to the surface side compared with that before the annealing, whereas the C profile after the higher-fluence HIBA has a more noticeable shift to the surface and a slight decrease in the concentration as well. This phenomenon may imply an effect of heat absorption of the target from the HIBA to cause loss of carbon probably due to the formation of hydrocarbon [18] which eases the evaporation. Comparing this result with that from 1000 °C thermal annealing which caused no change in the carbon profiles [18], we can realize that the HIBA, especially with higher fluences, makes the target absorb more heat and hence is more effective in annealing than the thermal techniques.

Since SiC nanocrystals have potential applications as nanoscale light emitters, luminescence from SiC crystallites has been experimentally studied for the crystallites fabricated with various methods [20]. However, we carried out PL measurements for the first time for the HIBA-crystallized SiC nanocrystals. The PL measurement results displayed in Fig. 6 show violet components in the range of 3.0–3.1, 3.2–3.35 and 3.4–3.5 eV [21,22]. All of the components are significantly enhanced after the Xe-HIBA, compared with the non-HIBA case. This fact indicates that the HIBA enhanced crystallization of SiC and thus the photoluminescence from the crystal. From the result we have noticed some features. First of all, the PL spectra have discontinuous separated, instead of continuous,

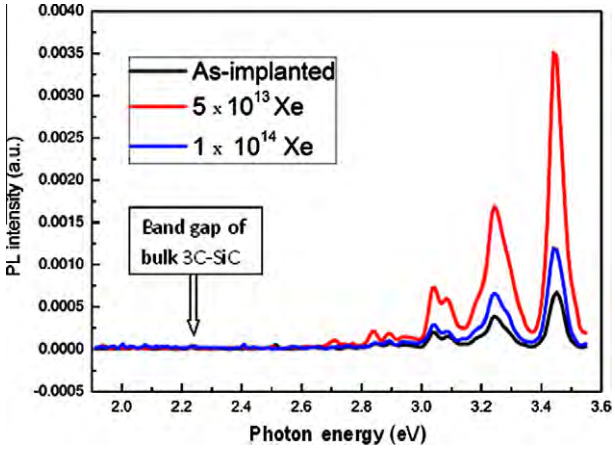

Fig. 6. PL spectra of SiC synthesized by 90-keV C-ion implantation in Si followed by 4-MeV Xe-ion beam annealing.

Table 1
Estimation of the SiC nanocrystal grain size distribution from the PL spectra in Fig. 6. PL: PL peak intensity in 10^{-4} according to the data in Fig. 6. PP: percentage of nanocrystal particles.

Photon energy (eV)	3.0–3.1	3.2–3.35	3.4–3.5
Particle size (nm)	6–7	4	3.5
5×10^{13} Xe-ions/cm^2	PL: 6	PL: 17	PL: 35
	PP: 10%	PP: 30%	PP: 60%
1×10^{14} Xe-ions/cm^2	PL: 2.5	PL: 6	PL: 12
	PP: 12%	PP: 30%	PP: 58%
As-C-implanted	PL: 2	PL: 4	PL: 7
	PP: 15%	PP: 30%	PP: 55%

peaks. This is a clear evidence of a quantum effect. Second, all the luminescence peaks are far higher in energy than the band gap of the bulk 3C–SiC as marked in the figure. This is clear evidence that the luminescence comes from SiC nanocrystals rather than bulk crystals because the quantum confinement effect can noticeably increase the band gap of SiC when the quantum dot size decreases down to nanometer scale [23]. From a gross estimation according to the transition energy as a function of particle size for porous SiC [24], the measured violet components mentioned above come from the SiC nanocrystals sized 6–7, 4, and 3.5 nm, respectively. Although the estimates may not be considered as very quantitative results due to the different conditions, the result qualitatively demonstrates a nanocrystal size distribution of SiC which is responsible for varied shorter-wavelength violet photoluminescence. Table 1 shows an estimate of the SiC nanocrystal size distribution calculated from the PL intensity by an assumption that the PL intensity is proportional to the number of the crystal particles. From the PL intensity distribution, we can see that the smallest nanocrystals are in the largest portion of all the nanocrystals. Third, all the violet components already exist for the as-implanted sample, although they are originally weak. This feature indicates that the C-ion implantation in Si at an elevated temperature can primarily form SiC nanocrystals but the number of the nanoparticles is smaller so that the PL intensity is lower. The HIBA crystallizes SiC nanocrystals, increases the number of the nanoparticles and thus the PL intensity increases. Fourth, the lower Xe-ion fluence (5×10^{13} ions/cm^2) gives the higher enhancement of the PL intensity than the higher fluence (1×10^{14} ions/cm^2). This might be because the higher fluence of the Xe-ion beam further increases the particle size and hence the number of the critically sized nanocrystals for the PL with the certain energies as mentioned above decreases.

4. Conclusion

SiC nanocrystals in Si single crystals could be synthesized by C-ion implantation in Si wafers followed by MeV HIBA. The technique has the following advantages: no need for a high annealing temperature, possibility of localized synthesis, easy control of the crystal size, and short time of treatment. The SiC nanocrystals synthesized by this technique could significantly enhance violet photoluminescence due to the quantum confinement effect.

Acknowledgments

This work was supported by the National Electronics and Computer Technology Center of Thailand, the National Research Council of Thailand, the Thailand Research Fund, the Thailand Center of Excellence in Physics, and the International Atomic Energy Agency (IAEA). J. Khamsuwan wishes to thank the scholarship from the Plasma Laboratory, City University of Hong Kong.

References

[1] Ioffe Physical Technical Institute, Russian Academy of Sciences, Electronic Archive: "New Semiconductor Materials: Characteristics and Properties", 2001. http://www.ioffe.ru/SVA/NSM/Semicond/SiC/.
[2] R. Madar, Nature 430 (2004) 974.
[3] S. Intarasiri, A. Hallén, A. Razpet, S. Singkarat, G. Possnert, Solid State Phenom. 107 (2005) 51.
[4] W. Wesch, Nucl. Instrum. Meth. B 116 (1996) 305.
[5] J.A. Borders, S.T. Picraux, W. Bcezhold, Appl. Phys. Lett. 18 (1971) 509.
[6] E. Theodossiu, H. Baumann, E.K. Polychroniadis, K. Bethge, Nucl. Instrum. Meth. B 161–163 (2000) 941.
[7] S. Intarasiri, L.D. Yu, S. Singkarat, A. Hallén, J. Lu, M. Ottosson, J. Jensen, G. Possnert, J. Appl. Phys. 101 (2007) 084311.
[8] A. Benyagoub, Nucl. Instrum. Meth. B 266 (2008) 2766.
[9] Z.J. Zhang, K. Narumi, H. Naramoto, S. Yamamoto, A. Miyashita, J. Phys. D Appl. Phys. 32 (1999) 2236.
[10] J.I. Langford, A.J.C. Wilson, J. Appl. Crystallogr. 11 (1978) 102.
[11] W. Wu, D.H. Chen, J.B. Xu, W.Y. Cheng, S.P. Wong, I.H. Wilson, R.W.M. Kwok, J. Vac. Sci. Technol. A 16 (3) (1998) 968.
[12] Y. Ito, T. Yamacuhi, A. Yamamoto, M. Sasase, S. Nishio, K. Yasuda, Y. Ishigami, Appl. Surf. Sci. 238 (2004) 159.
[13] S. Intarasiri, A. Hallén, J. Lu, J. Jensen, L.D. Yu, K. Bertilsson, M. Wolborski, S. Singkarat, G. Possnert, Appl. Surf. Sci. 253 (2007) 4836.
[14] Y.S. Katharria, S. Kumar, F. Singh, J.C. Pivin, D. Kanjilal, J. Phys. D Appl. Phys. 39 (2006) 3969.
[15] T. Zorba, D.I. Siapkas, C.C. Katsidis, Microelectron. Eng. 28 (1995) 229.
[16] J. Khamsuwan, S. Intarasiri, K. Kirkby, C. Jeynes, P.K. Chu, T. Kamwanna, L.D. Yu, Surf. Coat. Technol. (2011), doi:10.1016/j.surfcoat.2011.04.058.
[17] N.P. Barradas, C. Jeynes, R.P. Webb, Appl. Phys. Lett. 71 (1997) 291; Chris Jeynes, The IBA DataFurnace Homepage, 2005. http://www.ee.surrey.ac.uk/IBC/ndf/.
[18] S. Intarasiri, T. Kamwanna, A. Hallén, L.D. Yu, M.S. Janson, C. Thongleum, G. Possnert, S. Singkarat, Nucl. Instrum. Meth. B 249 (2006) 859.
[19] James F. Ziegler, SRIM–The Stopping and Range of Ions in Matter, in: Particle Interaction with Matter, 2009. http://www.srim.org/#SRIM.
[20] J.Y. Fan, X.L. Wu, P.K. Chu, Prog. Mater. Sci. 51 (2006) 983.
[21] K.H. Lee, S.K. Lee, K.S. Jeon, Appl. Surf. Sci. 255 (2009) 4414.
[22] J. Xu, L. Yang, Y.J. Rui, J.X. Mei, X. Zhang, W. Li, Z.Y. Ma, L. Xu, X.F. Huang, K.J. Chen, Solid State Commun. 133 (2005) 565.
[23] D.H. Feng, Z.Z. Xu, T.Q. Jia, X.X. Li, S.Q. Gong, Phys. Rev. B 68 (2003) 035334.
[24] J.S. Shor, L. Bemis, A.D. Kuttz, I. Grimberg, B.Z. Weiss, M.F. MacMillian, W.J. Choyke, J. Appl. Phys. 76 (1994) 7–4045.